Available online at www.sciencedirect.com

ScienceDirect

Advances in Space Research 56 (2015) 605–618

ADVANCES IN SPACE RESEARCH (a COSPAR publication)

www.elsevier.com/locate/asr

Influences of initial launch conditions on flight performance of high altitude balloon ascending process

Yi Zhang *, Dongxu Liu

School of Aeronautic Science and Engineering, Beijing University of Aeronautics and Astronautics, Beijing 100191, China

Received 2 December 2014; received in revised form 24 April 2015; accepted 27 April 2015
Available online 4 May 2015

Abstract

Influences of initial launch conditions on flight performance are addressed for the high altitude balloon ascending process. A novel dynamic model was established to describe thermodynamic and kinetic characteristics of balloon which consists of atmospheric, thermal and dynamic submodels. Based on the model, ascending processes of a high altitude balloon under different initial launch conditions were simulated. The initial launch conditions were classified into three types: inflating quantity, launch time and launch position. The ascending velocity and the differential pressure were defined and used as evaluation parameters of flight performance. Results showed that the inflating quantity is the most effective factor for ascending process, and the upper and lower limits were also proposed separately from safety and performance perspectives. For both launch time and launch location conditions, different solar radiation is the main effect approach during ascending process. Specifically, the influence mechanism of launch time in one day and launch longitude are completely identical due to the Earth's rotation. Results also showed that the sunset process is the optimal selection for safety of balloon and efficient utilization of solar energy. Due to the Earth's revolution, the influence mechanism of launch date and launch latitude are identical and the effects are more seasonal and less effective. Launch time and location should be considered comprehensively in practical operation of ballooning.

Keywords: High-altitude balloon; Flight performance; Launch conditions; Ascending process

1. Introduction

The high altitude balloon is a class of Lighter-than-air vehicle with application potential in communication, investigation, science exploration and other fields. Stratosphere is the most suitable space for the balloon because of year-long steady wind field in specific altitude (Schmidt et al., 2007). Therefore study in stratospheric balloon becomes the focus in many counties in recent years (Smith, 2004; Makino, 2002; Agrawal et al., 2002). In order to fulfill the tasks of a high altitude balloon, ascending process is an essential part of ballooning. During ascending, the lifting force is very sensitive to thermal effect (Palumbo et al., 2007). Both the balloon itself and the environment conditions affect ascending process (Guo and Zhu, 2013). Among those factors, launch conditions are of vital importance due to their controllability. To achieve better ascent performance, proper choices of launch conditions are required in the balloon mission preparation. On the other hand, poor launch conditions will cause potential safety risks and lead to the mission failure, especially for super-pressure balloons.

In the past decades, many important models of the performance of high altitude balloons have been developed. Kreith and Kreider (1974) provided an efficient and

* Corresponding author at: 1st South Keyan building, No. 37, Xueyuan road, Haidian district, Beijing 100191, China. Tel.: +86 10 82338480; fax: +86 10 82338481.
E-mail addresses: zhangyi@ase.buaa.edu.cn (Y. Zhang), liubuaa@163.com (D. Liu).

http://dx.doi.org/10.1016/j.asr.2015.04.031
0273-1177/

calibrated computer program to predict balloon ascent rates, ceiling, and behavior at float altitude which is considered as the starting point of the balloon modeling research. Carlson and Horn (1983) established a new thermal and trajectory model for high-altitude balloons, and the model predicted the temperature difference between gas and film which was observed in several test flights. The importance of thermal effect on balloon performance was revealed and more studies on radiative properties and thermal effect were completed (Cathey, 1996, 1997; Franco and Cathey, 2004) . Pankine et al. (2003) developed an advanced balloon performance and analysis tool called Navajo which can provide high-accuracy vertical and horizontal trajectory predictions. Farley (2005) built a new user-friendly software tool, in which adaptable formulations were generalized to allow balloon flight simulations in extraterrestrial atmospheres. Palumbo et al. (2007) constructed analysis code for high-altitude balloons including more features such as ballasting and valving, but is applied only to zero pressure balloons. The drag coefficient in the analysis code is presented as a function of the Reynolds number, the Froude number and another dimensionless parameter and it is quite suitable to fit the flight data. And based on the analysis code, a methodology was proposed for the prediction and optimization of the ascent trajectory (Morani et al., 2009; Palumbo et al., 2010). Conner and Arena (2010) discussed the development of a performance predictor for near space balloon systems and the balloon's volume and drag coefficient were established as a function of altitude. Dai et al. (2012) investigated the influence of film radiation properties and clouds on balloon thermal behaviors at float condition but the influence on ascending process was not discussed. Liu et al. (2014) proposed a novel model to investigate the thermal-dynamic performance of scientific balloon and the balloon film temperature distribution was discussed.

The foregoing articles mainly focused on the accuracy and correctness of the model to make the prediction more accurate. The effects of launch conditions on balloon flight performances have not been given much attention. The primary purpose of this study is to reveal the influence mechanism of launch conditions on flight performance through modeling of high altitude super-pressure balloon. The remainder of this paper is organized as follows. In Section 2, features and hypothesis of high altitude balloon are introduced firstly to build a balloon flight simulation model. Then, submodels of atmosphere, thermal effect and dynamics are established and governing equations are presented. Section 3 describes the simulation method which includes simulation environment, initial launch conditions and evaluation parameters. Finally, the accuracy of the model is verified by comparing the simulation data to the measured data. After validation the numerical solution is given under different launch conditions. Based on the simulation results, influence of launch conditions are discussed.

2. High altitude balloon model

The object of the model is a super-pressure balloon made of a composite fabric that is filled with helium. The pressure inside the envelop is maintained above the ambient pressure at all times to keep the balloon afloat at a constant altitude. Based on the general model of fixed-wing aircraft, some specific features were introduced into the high altitude balloon model. These features include high-altitude thermal radiation environment, buoyancy, virtual mass and the coupling relation between kinetics and thermodynamics. And in order to simplify the model, some reasonable hypothesis are made:

- The system of high altitude balloon is treated as rigid body in kinetic equations.
- In the ascent phase, the shape of the balloon is always assumed to be spherical.
- The temperature of balloon film and helium inside are both represented as arithmetic average value.

2.1. Atmospheric model

The atmosphere model in this paper consist of atmospheric parameters which are only related to geopotential altitude. The model implements the mathematical representation of the 1976 Committee on Extension to the Standard Atmosphere (COESA) United States standard lower atmospheric values for absolute temperature, pressure and density for the input geopotential altitude.

2.2. Thermal model

Stratospheric balloon thermodynamic models are used to calculate the temperature both of the balloon film and the internal helium. Factors that affect the temperature variations include environmental radiation, thermal characteristics of the balloon film, convective heat transfer, and the expansion and compression of balloon as a result of the state change of helium. Fig. 1 describes the components of thermal behaviors. These factors vary with time, location, altitude, weather, the amount of helium gas and the parameters of balloon. Therefore, a thermodynamic model which can adapt to complex flight state is necessary for evaluating the influence of launch conditions on the flight performance of stratospheric balloon.

2.2.1. Environment radiation

Environment radiation in flight includes direct solar radiation, solar scattering radiation, planet albedo radiation, cloud layer albedo radiation and planet infrared radiation.

2.2.1.1. Direct solar radiation. Of all the sources of radiation received by a balloon, the direct solar radiation is the most critical. There are many factors that affect the direct

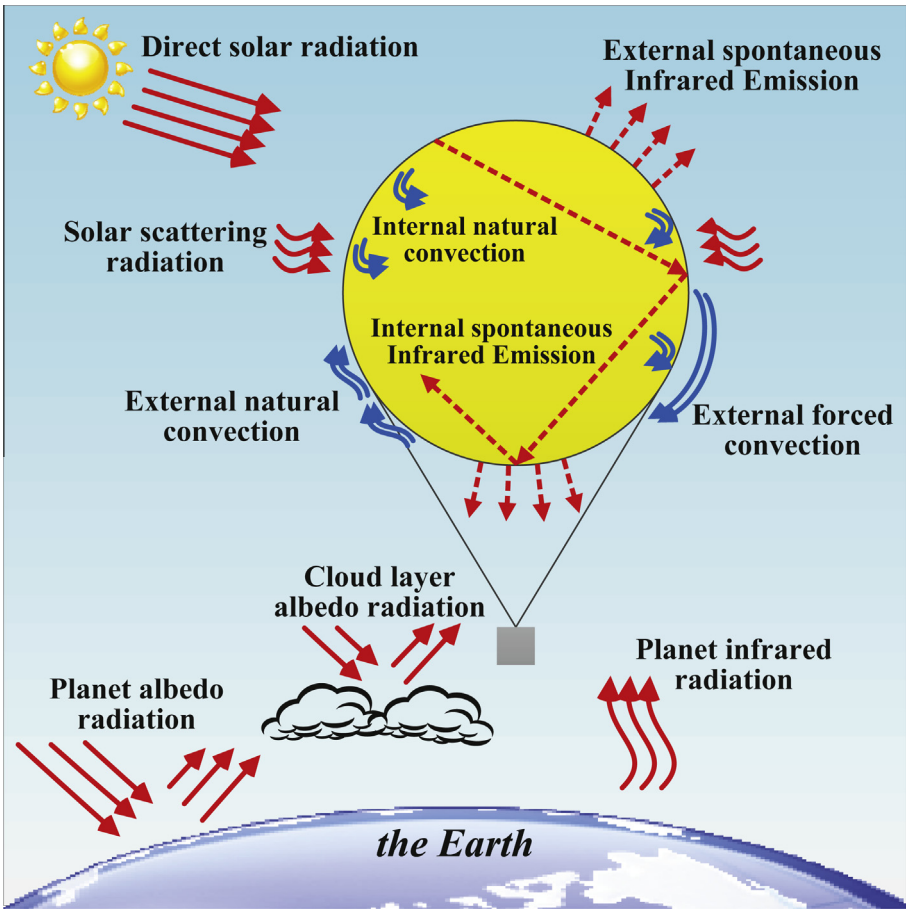

Fig. 1. High altitude balloon thermal environment.

solar radiation arriving at a high-altitude balloon (Ran et al., 2007). These factors can be divided into two groups. The first group includes a single factor, the day of year, which determines the intensity of the extraterrestrial normal solar radiation. The 2nd group of parameters determines the actual intensity of the direct solar irradiation on the balloon. This includes attenuation effect of atmospheric, time of day, altitude of balloon, operating latitude and longitude. The weakening effect of the atmosphere can be measured by transmittance factor. Simultaneously, considering the effect of cloud layer, the power of direct solar radiation on balloon can be divided into two cases:

$$I_{sunD} = \begin{cases} C_{cv} \cdot I_{sun} \cdot \tau_{atm} & \text{if } h \leqslant h_c, \\ I_{sun} \cdot \tau_{atm} & \text{if } h > h_c. \end{cases} \tag{1}$$

where h is the altitude of balloon, h_c represents cloud height and the subscript 'c' means cloud, C_{cv} is the transparency coefficient of cloud, which is divided into three cases according to the thickness of cloud: $C_{cv} = 1$ when there is no cloud, $C_{cv} = 0.5$ when cloud is thin, $C_{cv} = 0.1$ when cloud is thick. I_{sun} and τ_{atm} are the intensity of the extraterrestrial normal solar radiation and the transmittance factor of the atmosphere, respectively (Farley, 2005; Germeles, 1966). And the subscript '*atm*' means atmosphere.

$$I_{sun} = \frac{I_{sc}}{R_{AU}^2} \cdot \left(\frac{1 + e_{earth} \cdot \cos TA}{1 - e_{earth}^2} \right)^2, \tag{2}$$

$$\tau_{atm} = \begin{cases} 0 & \text{if } SE \leqslant DIP, \\ \dfrac{(exp(-0.65R_{AM}) + exp(-0.095R_{AM})) \cdot \left(1 + 0.4\left(\frac{P_{air}}{P_0}\right)^2\right)}{2} & \text{if } SE > DIP. \end{cases} \tag{3a}$$

$$R_{AM} = \frac{P_{air}}{P_0} \left[\sqrt{1228.6 + (613.8 \sin SE)^2} - 613.8 \sin SE \right], \tag{3b}$$

where I_{sc} is the (extraterrestrial normal) solar radiation constant which is defined as the rate of total solar energy at all wavelengths incident on a unit area exposed normally to rays of the Sun at the mean Sun–Earth distance and $I_{sc} = 1358\ \mathrm{W/m^2}$ (Ran et al., 2007; Farley, 2005). R_{AU} and e_{earth} are parameters related to the planet, as for the Earth, $R_{AU} = 1$ and $e_{earth} = 0.016708$. TA represents the true anomaly, which is obtained from day number of the year, ranging from 1 on January 1 to 365 on December 31. SE and DIP are sun elevation angle and the angle between the true horizon and the apparent horizon, which are shown in Fig. 2. R_{AM} is the air mass ratio

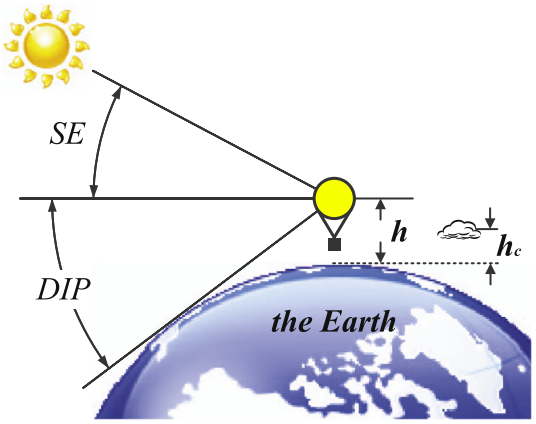

Fig. 2. Position relation of Sun, Earth and balloon.

which is related to the altitude of balloon h and the sun elevation angle SE (Germeles, 1966). P_{air} and P_0 are both air pressure, the former is the pressure at the altitude of balloon and the latter is sea level pressure.

2.2.1.2. Solar scattering radiation. The solar scattering radiation changes with I_{sun}. Replacing τ_{atm} by scattering transmittance factor τ_{sc}, the power of solar scattering radiation is as follows:

$$I_{sunS} = I_{sun} \cdot \tau_{sc}. \tag{4}$$

Here, τ_{sc} is related to the altitude of balloon and SE. The computational formula is as follows (Ran et al., 2007; Dai et al., 2012):

$$\tau_{sc} = \begin{cases} 0 & \text{if } SE \leqslant 0, \\ 0.2e^{-\frac{h}{10000}} \sin SE & \text{if } SE > 0. \end{cases} \tag{5}$$

Here, 10,000 is a relative altitude and the unit is m.

2.2.1.3. Planet albedo radiation. The planet albedo radiation refers to the reflected radiation by earth surface after passing through the atmosphere to the ground. Considering the effect of cloud layer, the power of planet albedo radiation on balloon is divided into two cases:

$$I_{sunE} = \begin{cases} C_{cv} \cdot \rho_{ev} \cdot I_{sun} \cdot \tau_{atm} \cdot \sin SE & \text{if } h \leqslant h_c, \\ C_{cv}^2 \cdot \rho_{ev} \cdot I_{sun} \cdot \tau_{atm} \cdot \sin SE & \text{if } h > h_c, \end{cases} \tag{6}$$

where ρ_{ev} is reflectance coefficient of earth surface to visible light.

2.2.1.4. Cloud layer albedo radiation. If the cloud thickness is deep and the balloon is higher than cloud layer, a part of visible light will be reflected by cloud to the balloon. The power of cloud layer albedo radiation is as follows:

$$I_{sunC} = \begin{cases} 0 & \text{if } h \leqslant h_c, \\ (1 - C_{cv}) \cdot I_{sun} \cdot \tau_{atm} \cdot \sin SE & \text{if } h > h_c. \end{cases} \tag{7}$$

2.2.1.5. Planet infrared radiation. The earth and the surrounding atmosphere as a whole forms the main source of planet infrared radiation. Due to the lack of the solar radiation at night, the effects of planet infrared radiation on balloon is stronger than during the day. In the atmosphere, water and carbon dioxide have a relatively high impact on infrared radiation, and the influence degree is different in different wavelength region (Cho and Raque, 2002). Therefore, the power of planet infrared radiation is obtained through integration in different wavelength range by comparing the altitude of balloon h with the altitude h_{h2o} and h_{co2} at which water and carbon dioxide are centralized in the atmosphere.

$$I_{eIR} = \begin{cases} \begin{cases} I(\lambda, T_{air}) & \text{if } h < h_{h2o} \\ I(\lambda, T_{air,h2o}) & \text{if } h \geqslant h_{h2o} \end{cases} & 3 \times 10^{-6} \leqslant \lambda < 8 \times 10^{-6} \\ \begin{cases} I(\lambda, T_g) & \text{if } h < h_c \\ C_{ci} \cdot I(\lambda, T_g) & \text{if } h \geqslant h_c \end{cases} & 8 \times 10^{-6} \leqslant \lambda < 9.4 \times 10^{-6} \\ I(\lambda, T_{air}) & 9.4 \times 10^{-6} \leqslant \lambda < 9.8 \times 10^{-6} \\ \begin{cases} I(\lambda, T_g) & \text{if } h < h_c \\ C_{ci} \cdot I(\lambda, T_g) & \text{if } h \geqslant h_c \end{cases} & 9.8 \times 10^{-6} \leqslant \lambda < 13 \times 10^{-6} \\ \begin{cases} I(\lambda, T_{air}) & \text{if } h < h_{co2} \\ I(\lambda, T_{air,co2}) & \text{if } h \geqslant h_{co2} \end{cases} & 13 \times 10^{-6} \leqslant \lambda < 17 \times 10^{-6} \\ \begin{cases} I(\lambda, T_{air}) & \text{if } h < h_{h2o} \\ I(\lambda, T_{air,h2o}) & \text{if } h \geqslant h_{h2o} \end{cases} & 17 \times 10^{-6} \leqslant \lambda < 50 \times 10^{-6} \end{cases}, \tag{8}$$

where T_{air}, $T_{air,h2o}$ and $T_{air,co2}$ represent atmospheric temperature at balloon altitude h, water altitude h_{h2o} and carbon dioxide altitude h_{h2o}, respectively. The subscript '$h2o$' and '$co2$' means water and carbon dioxide, respectively. And $I(\lambda, T)$ is the Blackbody Radiation Law as follows:

$$I(\lambda, T) = \frac{2hc^2}{\lambda^5} \frac{1}{e^{\frac{hc}{\lambda kT}} - 1}. \tag{9}$$

2.2.2. Balloon film

The balloon's skin temperature is mainly affected by the environment radiation, its infrared emission and the internal and external convective heat transfer.

2.2.2.1. Radiant heat loads on the film. After certain amount of radiation is absorbed by the skin, the rest will be sent to other places by reflection and transmission. The proportion of three parts is decided by the absorptivity, emissivity and transmissivity factors of skin material. Due to the different radiation angle of environmental radiation, irradiation area of each kind of radiation needs to be calculated. The direct solar radiation is considered as parallel light, the effective area that receive radiation can be obtained from the radius of balloon.

$$A_{top} = \pi R^2. \tag{10}$$

As for solar scattering radiation, the exposed area of balloon needs to be calculated.

$$A_{surf} = 4 \cdot \pi R^2. \tag{11}$$

As for planet albedo radiation, cloud layer albedo radiation and planet infrared radiation, a view factor is needed on the basis of exposed area, which is obtained as follows:

$$F_{view} = \frac{1 - \cos\left(\frac{\pi}{2} - DIP\right)}{2}. \tag{12}$$

After transmission, environmental radiation will produce multiple reflections inside balloon. An effective reflectivity value is obtained as a result of multiple reflections accumulation (including visible light and infrared light).

$$r_e = r + r^2 + r^3 + r^4 + r^5 + \cdots, \tag{13}$$

$$r_{e,IR} = r_{IR} + r_{IR}^2 + r_{IR}^3 + r_{IR}^4 + r_{IR}^5 + \cdots, \tag{14}$$

where r and r_{IR} are reflective factors of balloon film to visible light and infrared radiation, respectively. The subscript '*IR*' means infrared radiation. So far every part of radiation absorption is obtained. Direct solar radiation:

$$Q_{sunD} = \alpha \cdot I_{sunD} \cdot A_{top} \cdot [1 + \tau(1 + r_e)], \tag{15}$$

where α and τ are absorptance factor and transmittance factor of balloon film to visible light. Solar scattering radiation:

$$Q_{sunS} = \alpha \cdot I_{sunS} \cdot A_{surf} \cdot [1 + \tau(1 + r_e)]. \tag{16}$$

Planet albedo radiation:

$$Q_{sunE} = \alpha \cdot I_{sunE} \cdot A_{surf} \cdot F_{view} \cdot [1 + \tau(1 + r_e)]. \tag{17}$$

Cloud layer albedo radiation:

$$Q_{sunC} = \alpha \cdot I_{sunC} \cdot A_{surf} \cdot F_{viewc} \cdot [1 + \tau(1 + r_e)], \tag{18}$$

where F_{viewc} is a view factor of cloud layer which is obtained from Eq.(12) by replacing *DIP* with DIP_c. DIP_c is the angle to the surface of the cloud while *DIP* is the angle to the surface of the earth. Planet infrared radiation:

$$Q_{eIR} = \alpha_{IR} \cdot I_{eIR} \cdot A_{surf} \cdot F_{view} \cdot [1 + \tau_{IR}(1 + r_{e,IR})], \tag{19}$$

where α_{IR} and τ_{IR} are absorptance factor and transmittance factor of balloon film to infrared radiation.

2.2.2.2. Spontaneous infrared emission of film. The spontaneous infrared emission of film can be divided into two parts. The first one is infrared radiation of both sides of surface transmitted to the external environment, which is in accordance with the Blackbody Radiation Law:

$$Q_{fIRout} = 2 \cdot \sigma \cdot \varepsilon_{IR} \cdot A_{surf} \cdot T_{film}^4, \tag{20}$$

where σ is the Boltzmann constant, ε_{IR} is the infrared emittance factor of balloon film and T_{film} is the temperature of balloon film. The other part is the reabsorption of inner surface from infrared emission, and after the process of multiple reflections, the reabsorption part is as follows:

$$Q_{fIRin} = \alpha_{IR} \cdot \sigma \cdot \varepsilon_{IR} \cdot A_{surf} \cdot T_{film}^4 \cdot (1 + r_{e,IR}). \tag{21}$$

2.2.2.3. Convective heat loads on the film. The convective heat loads on the film consists of two parts. One is the convection heat between outer surface and surrounding air, and the other is the convection heat between inner surface and the helium inside. Due to the relative motion between balloon and ambient air during ascent, convective heat transfer performance can be divided into two types depending on the size of the relative velocity: natural convection and forced convection (Carlson and Horn, 1983). The movement of helium inside balloon is relatively stable, therefore only natural convection is considered when dealing with inner convection heat in the model. The natural convection heat transfer coefficient between external skin and air:

$$HC_{free} = \frac{Nu_{air} \cdot k_{air}}{d}, \tag{22}$$

where Nu_{air} and k_{air} are Nusselt number and thermal conductivity of the air, respectively. d is the diameter of balloon. The forced convection heat transfer coefficient between external skin and air (Farley, 2005):

$$HC_{force} = \frac{k_{air}}{d} \cdot (2 + 0.41 \cdot Re^{0.55}), \tag{23}$$

where *Re* is the Reynolds number based on the length of the balloon diameter. The larger one between two coefficients above-mentioned is selected to calculate the convective heat loads on the external film.

$$Q_{HCex} = max(HC_{free}, HC_{force}) \cdot A_{surf} \cdot (T_{air} - T_{film}). \tag{24}$$

The natural convection heat transfer coefficient between internal skin and helium (Farley, 2005):

$$HC_{in} = 0.13 \cdot k_{he} \cdot \left(\frac{\rho_{he}^2 \cdot g \cdot |T_{film} - T_{he}| \cdot Pr_{he}}{T_{he} \cdot \mu_{he}^2}\right)^{\frac{1}{3}}, \tag{25}$$

where $k_{he}, \rho_{he}, T_{he}, Pr_{he}$ and μ_{he} are thermal conductivity, density, temperature, the Prandtl number and coefficient of kinetic viscosity of helium, respectively. The convective heat load on the internal film:

$$Q_{HCin} = HC_{in} \cdot A_{surf} \cdot (T_{he} - T_{film}). \tag{26}$$

Considering the environmental radiation, infrared spontaneous emission and convective heat transfer, the rate of temperature change of balloon film can be obtained as follows:

$$\frac{dT_{film}}{dt} = \frac{Q_{sunD} + Q_{sunS} + Q_{sunE} + Q_{sunC} + Q_{eIR} - Q_{fIRout} + Q_{fIRin} + Q_{HCex} + Q_{HCin}}{c_f \cdot m_f}, \tag{27}$$

where c_f and m_f are specific heat capacity and mass of balloon film.

2.2.3. Helium

The change of helium temperature is mainly affected by its own expansion and compression and convective heat transfer between the skin and helium. During ascent and descent phase of flight, the change of the atmospheric

pressure will cause adiabatic expansion and compression of balloon. Due to the inner helium is in closed environment, the intensity of natural convection heat transfer between the helium and the inner skin is low. Therefore, the expansion and compression of helium can be considered as adiabatic process. As internal convective heat transfer has been given in Eq. (26), the rate of temperature change of helium can be obtained as follows:

$$\frac{dT_{he}}{dt} = \frac{-Q_{HCin}}{c_v \cdot m_{he}} + (\gamma - 1) \cdot T_{he} \cdot \left(\frac{dm_{he}}{dt} \cdot \frac{1}{m_{he}} - \frac{dV_{he}}{dt} \cdot \frac{1}{V_{he}} \right), \tag{28}$$

where c_p and c_v are the specific heat of helium at constant pressure and constant volume. And γ is the ratio of these two parameters, $\gamma = c_p/c_v$.

2.3. Dynamic model

2.3.1. Reference frames

Referring to the modeling of conventional fixed-wing aircraft, the earth and body reference frames should be defined first. The earth reference frame (ERF) is fixed to the earth with its origin O_g located at launch point of balloon on the ground. The $O_g x_g$ axis points to the north, the $O_g y_g$ axis points to east and the $O_g z_g$ axis points to the earth core. The body reference frame (BRF) is attached to the balloon with its origin O coincident with the center of volume. Because the balloon is in centrosymmetric structure, the O_x axis points to the head of the balloon with any fixed point on the equator of balloon. The O_z axis is perpendicular to the O_x axis and points to downwards. The O_y axis is determined by the right-hand rule and points to starboard.

2.3.2. Forces on balloon

The external forces applied to the balloon include gravity, buoyancy, aerodynamic force and added inertia force. Here, the added inertia forces are treated as virtual mass and inertia (Mueller et al., 2004).

2.3.2.1. Buoyancy. The lifting force that allows a balloon to rise is total buoyancy which derives from the Archimedes' principle.

$$B = \rho_{air} \cdot g \cdot V_{he}. \tag{29}$$

2.3.2.2. Gravity. The mass of the high altitude balloon system is constructed by several parts: film, helium, cabin, load and ballast, all above should be taken into account in the calculation of gravity. The total gravity is defined by:

$$G = (m_f + m_{he} + m_c + m_l + m_b) \cdot g. \tag{30}$$

Here the m_f, m_{he}, m_c, m_l and m_b denotes the mass of film, helium, cabin, load and ballast, respectively.

2.3.2.3. Aerodynamic force. Unlike conventional aircraft that rely on aerodynamic force as the main source of lift, balloon depends on buoyancy more during flight. Besides, the shape of balloon is axially symmetric whether in overpressure state or not. Therefore the aerodynamic drag is mainly considered in the model. The formulas of aerodynamic drag in three directions are given by:

$$\begin{cases} D_x = \frac{1}{2} \cdot C_{Dx} \cdot \rho_{air} \cdot u^2 \cdot S, \\ D_y = \frac{1}{2} \cdot C_{Dy} \cdot \rho_{air} \cdot v^2 \cdot S, \\ D_z = \frac{1}{2} \cdot C_{Dz} \cdot \rho_{air} \cdot w^2 \cdot S, \end{cases} \tag{31}$$

where C_{Dx}, C_{Dy} and C_{Dz} are aerodynamic drag coefficients in three directions, respectively. And they are assumed to be constant in the model (Farley, 2005), that is $C_{Dx} = C_{Dy} = C_{Dz} = 0.8$. S is reference area of balloon, which is generally described as $S = V^{2/3}$. u, v and w are airspeed in directions of x, y and z axis of body reference frame.

2.3.3. Dynamic equations

According to above mechanical analysis, the dynamics equations of high altitude balloon in body reference frame are established as follows:

$$\begin{cases} \dot{u} \cdot (m + m_{add}) = D_x, \\ \dot{v} \cdot (m + m_{add}) = D_y, \\ \dot{w} \cdot (m + m_{add}) = B + G + D_z, \end{cases} \tag{32}$$

where m is the overall mass of the balloon system (including the helium), m_{add} is the virtual mass. And for the balloon, $m_{add} = 0.5\rho_{air} V_{he}$ (Anderson and Taback, 1991).

3. Simulation method

Based on the high altitude balloon model, simulation platform is built in the Matlab/Simulink environment. The simulation program consists of a main program and two subroutines handling thermodynamic equations and kinetic equations, respectively. And differential equation solver 'ode45' in Matlab/Simulink is used to solve the second order differential equations described in the Section 2. A complete program flow chart is shown in Fig. 3.

3.1. Initial conditions

The influence of inflating quantity, launch time and launch position on the flight performance of high altitude balloon were studied respectively.

Inflating quantity refers to the total helium mass inflated into the balloon before launch. Inflating quantity directly affect the rising velocity of balloon during ascending, and the velocity increases with larger inflating quantity. However, excessive inflating quantity will result in larger differential pressure after overpressure.

Generally, inflating quantity is proportional to design volume of the balloon. Without loss of generality, we defined the following two concepts: 'design inflating quantity' and 'inflating multiples'. Design inflating quantity

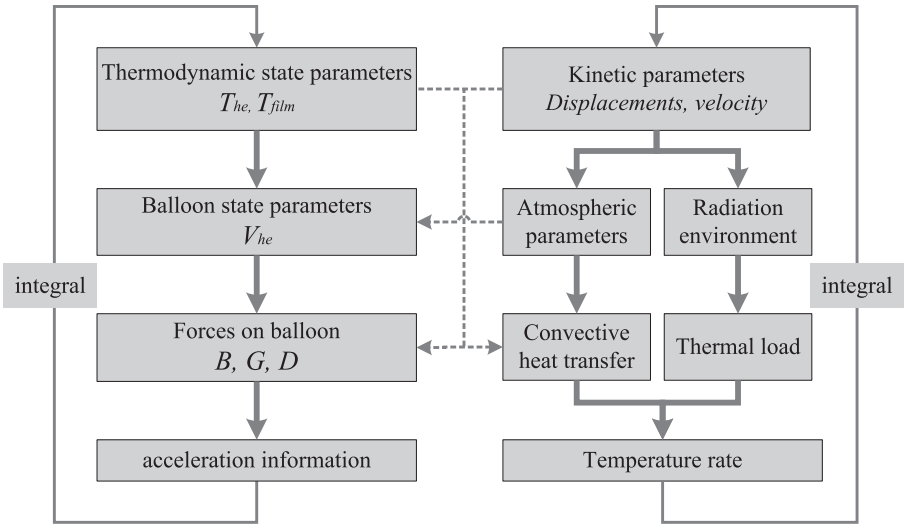

Fig. 3. Flow chart of the simulation platform.

indicates the mass of helium under which the balloon will maintain not only maximum overall shape but zero differential pressure at float altitude. Actually, design inflating quantity m_{he0} is the minimum helium mass which can make the balloon float at the desired altitude. Considering the aerodynamic drag and the temperature drop caused by expansion during ascent, more helium than m_{he0} is needed to provide free-lift. Inflating multiples N_{he} indicates the ratio of real helium mass m_{he} that inflated into the balloon before launch to design inflating quantity m_{he0}. So $N_{he} = m_{he}/m_{he0}$ and $(N_{he} - 1)m_{he0}$ is the amount of extra helium to drive the balloon upward.

Because of the relationship between solar radiation intensity and time of flight, launch time can affect the ascent phase of balloon. The influence of the launch time on flight performance was analyzed in simulation process from two aspects. One is from the perspective of longer interval, the season in which the balloon launch is the main factor to be considered. The other is from the perspective of shorter interval, different launch time of one day is the main factor to be considered.

Launch position refers to the latitude and longitude of launch site. Launch position affects the flight performance through different solar radiation intensity. The influence of latitude and longitude were analyzed separately.

3.2. Performance parameters in ascent phase

Performance parameters of balloon in flight include position, velocity, attitude, temperature, pressure and other aspects. For the ascent phase, rise velocity, film temperature and differential pressure between internal and external of balloon are most concerned by designer and operator. The film temperature must not drop below the cold brittle point of the film otherwise the balloon will burst especially when dealing with high values of gas mass. However, the cold brittle temperatures of the film differ according to the materials which the film are composed of. And considering sudden film temperature drops are always caused by large vertical velocities, so rise velocity and differential pressure were selected as performance evaluation index in simulation and analysis. Here, average rate of climb was defined as the mean value of rising velocity in the period from launch to expanding to design volume. And maximum differential pressure is defined as the maximum value of differential pressure at the end of ascent phase.

4. Results and discussion

4.1. Model validation

The accuracy of the model introduced in this paper is evaluated by comparison with the experimental results of a NASA super pressure balloon flight which was flown on June 22, 2008 from Ft. Sumner, New Mexico (Cathey, 2009). This test flight balloon had a volume of 26790 m^3 and was designed to float at an altitude of 30.5 km with a suspended load of 295 kg. The launch took place at 7:18 AM local time, and after a nominal ascent, the balloon began to pressurize when it reached a steady float altitude of 30.5 km. A total of 109 kg of ballast was then dropped in several increments to adjust the altitude and challenge a higher differential pressure value.

This flight has been analyzed with the present program using the model developed in this paper. It is assumed that the surrounding atmosphere environmental is standard atmosphere with clear sky and the launch site is 34°28′N, 104°14′W. By comparing the predicted results with the flight data, the validity and accuracy of the present model can be obtained.

Figs. 4 and 5 compare the altitude predictions with the flight data for the entire flight (not including descent) and for the 'at float' portion of the flight. The flight data and the predicted data from present model agree with each

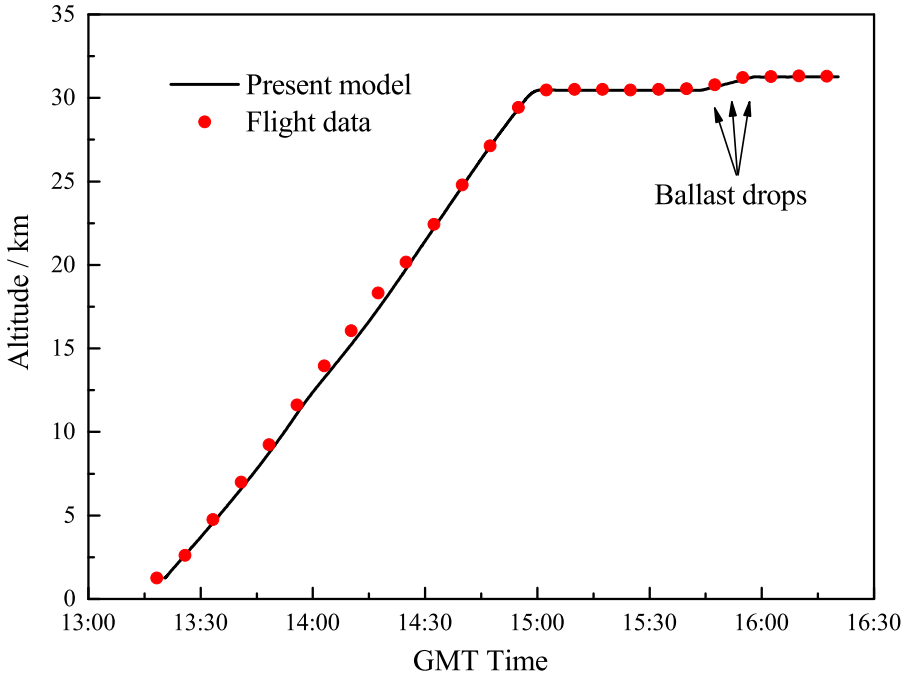

Fig. 4. Altitude comparison of the predicted data with the measured data – entire flight.

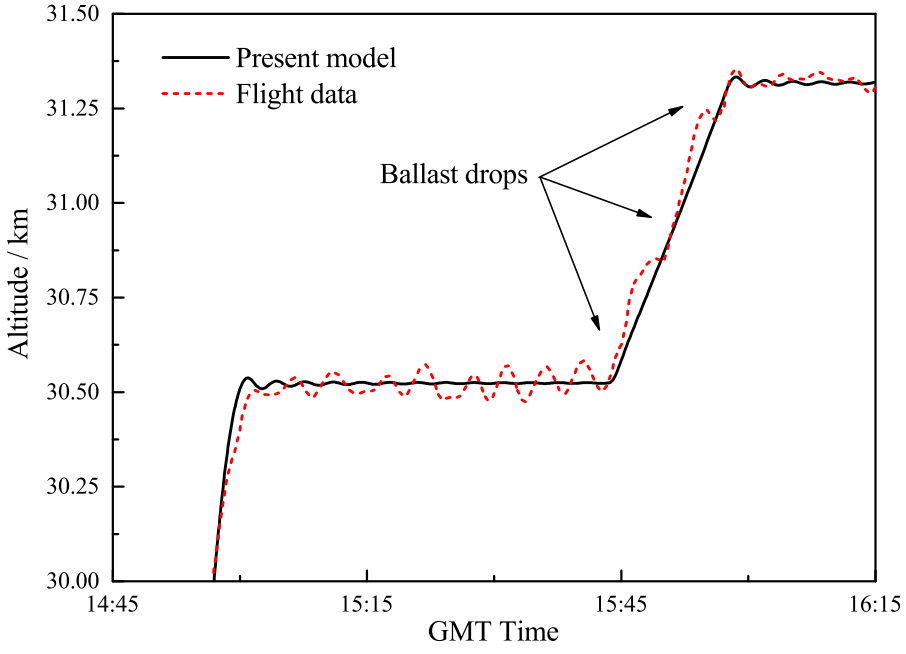

Fig. 5. Altitude comparison of the predicted data with the measured data – float.

other well. It should be noted that in the ascending process there exist some discrepancy between them. The assumption of aerodynamic drag coefficient may be the main factor caused that discrepancy. Considering the drag coefficient as constant made the curve of predicted data more straight. And in float phase the two sets of data agree better with each other in Fig. 5 as a result of the decrease of influence from drag force. Fig. 6 compares the predicted differential pressures with the measured data and they matched well with each other in trend. And the effects of ballast drops on altitude in Fig. 5 and differential pressures in Fig. 6 were presented accurately.

4.2. Influence of launch conditions

After validation of the model, the influences of launch conditions on flight performance of a high altitude super-pressure balloon were investigated. The design

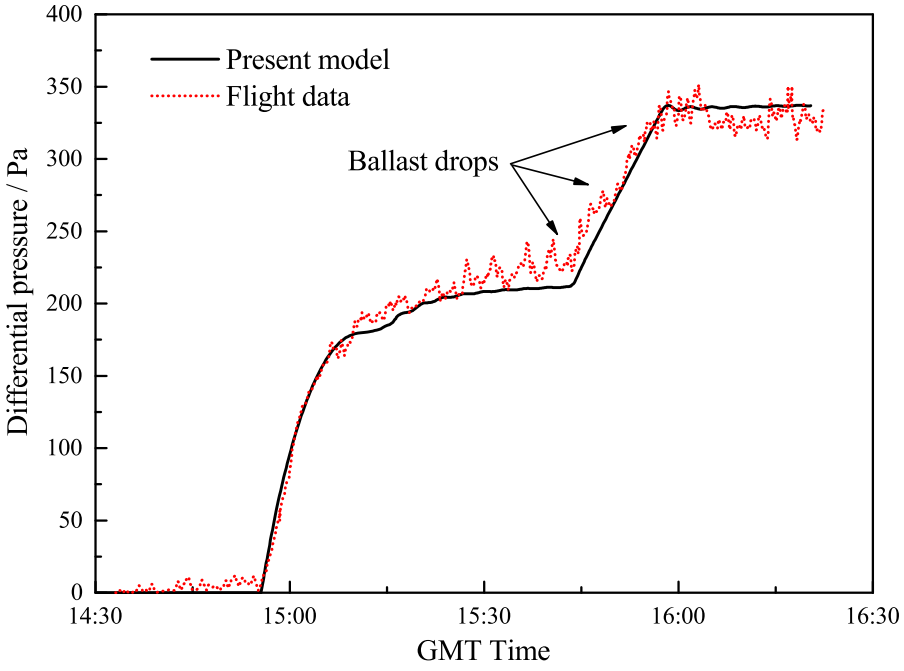

Fig. 6. Differential pressure comparison of the predicted data with the measured data.

parameters of the balloon are presented in Table 1 and these parameters are universal in all cases. The launch conditions are presented in Table 2 and in every simulation case one specific parameter is expanded to investigate the influence on flight performance.

4.2.1. Influence of inflating quantity

Because the balloon has to pass the gales area during ascending, a bigger rate of climb is always expected to avoid excessive lateral displacement. Increasing the inflating quantity is the most efficient way to obtain faster climbing speed. The influence of inflating quantity on rate of climb is shown in Fig. 7. The curves of climbing rate are smooth during ascending except a "cusp" at altitude of 11 km which is caused by the discontinuity of atmospheric density ρ_{air}. It is obviously that larger inflating quantity can provide greater rising speed. When inflating multiples N_{he} is set to 1.1, the duration of whole ascent process last two hours. However when N_{he} is set to 1.25, the duration was shortened to 1 h and 5 min.

On the other hand, excessive inflating quantity also caused the excessive differential pressure which will challenge the strength of balloon film. Variations of average climb rate and maximum differential pressure with respect to inflating multiples are shown in Fig. 8. The linear relationship between differential pressure and mass of helium is demonstrated in Fig. 8. On the other hand, although buoyancy shows a linear variation with the helium mass, since aerodynamic drag is proportional to the square of rising speed, the average rate of climb had a nonlinear relationship with the inflating multiples.

The above results showed that selection of the inflating multiples should take into consideration both the rising speed and maximum differential pressure. The lower bound of inflating multiples is determined by acceptable minimum rising speed. And the upper bound is determined by both rising speed and the maximum differential pressure the balloon can withstand. Either the excessive differential pressure or the film temperature drops caused by excessive rising velocity will lead to burst of balloon. The optimal value of inflating multiples must lie within this range.

Table 1
Parameters of the high altitude super-pressure balloon.

Design parameter	Value
Maximum volume V_{max}, m^3	14,137
Diameter d, m	30
Design inflating quantity m_{he0}, kg	172
Total weight (helium not included), kg	1073
Float altitude h, km	20
Cloud condition	No cloud
Absorptivity of film α	0.13
Transmissivity of film τ	0.03
Absorptivity of film for IR α_{IR}	0.7
Transmissivity of film for IR τ_{IR}	0.1

Table 2
Launch conditions in simulation cases.

Design parameter	Value
Inflating multiples N_{he}	1.2
Launch position	40°N, 116°E
Launch time	12 AM local time
Launch date	September 4, 2012

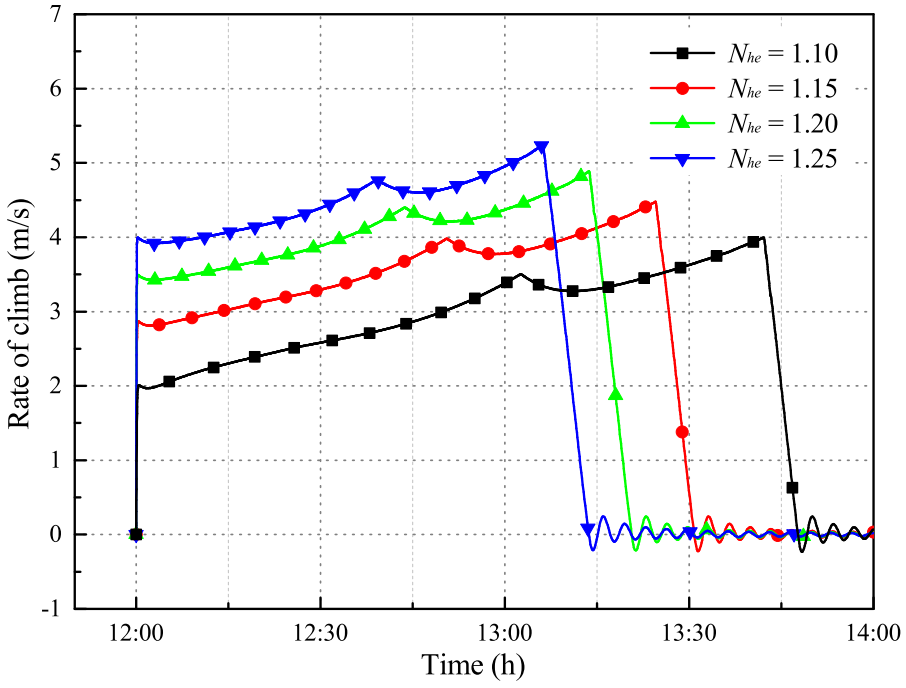

Fig. 7. Rate of climb with different N_{he} versus time.

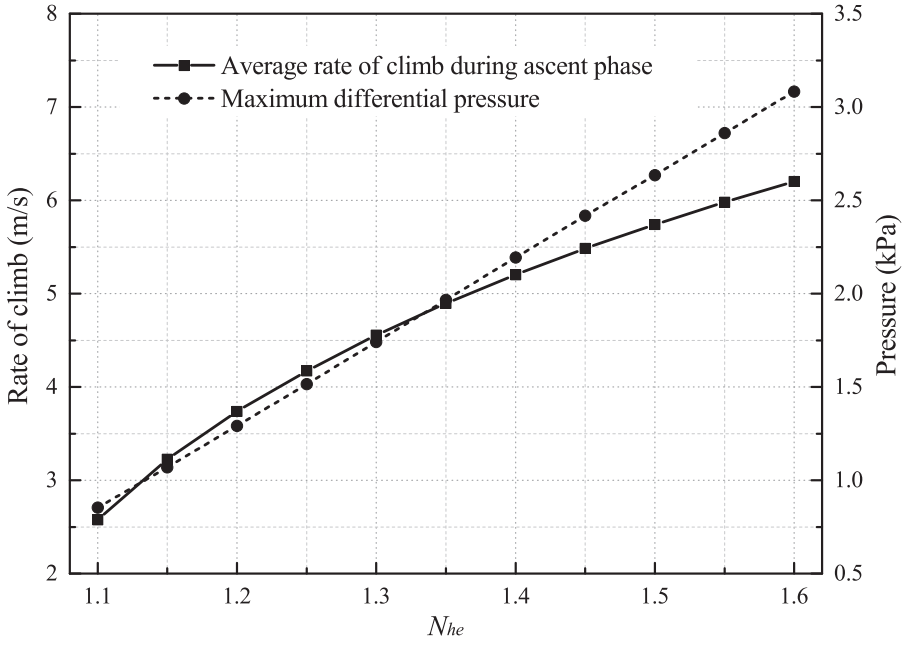

Fig. 8. Average rate of climb and maximum differential pressure versus N_{he}.

4.2.2. Influence of launch time

Fig. 9 presents the average rate of climb and the maximum differential pressure during ascent phase at different launch time in 24 h. The variations of two parameters show relatively consistent trend with each other. It is obvious that both the rising speed and the maximum differential pressure are larger in the daytime than at night. The values of two parameters maintain at a lower level, begin to increase from early in the morning (at about 6:00 am) and reach the peak at midday. Subsequently, they gradually decrease and return to the lowest level in evening (at about 8:00 pm). It is in good agreement with the variation of direct solar radiation intensity in one day when comparing Figs. 9 and 10, which illustrates that the direct solar radiation is the main factor through which the ascent phase is influenced by launch time. Because of the average rising

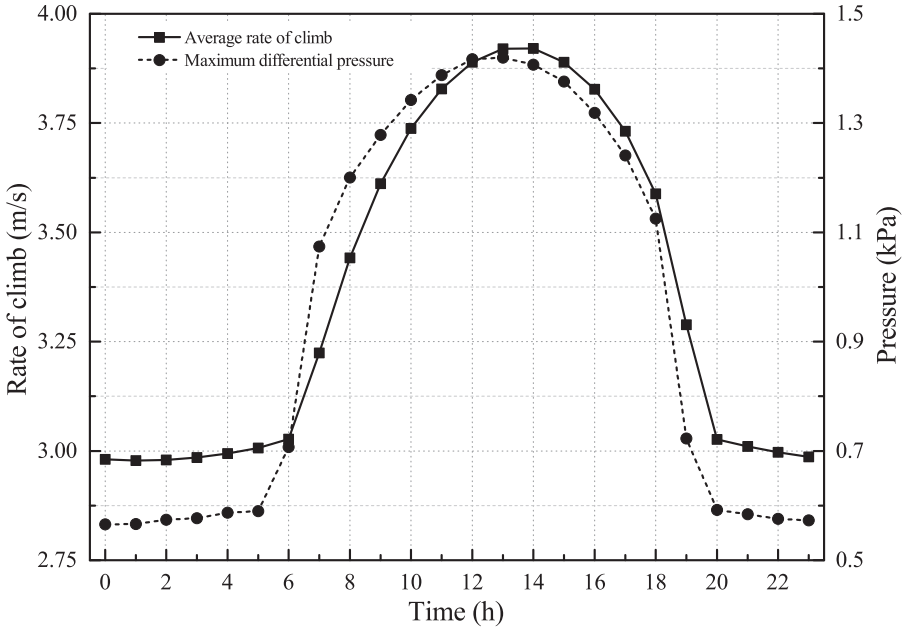

Fig. 9. Average rate of climb and maximum differential pressure at different launch time in one day.

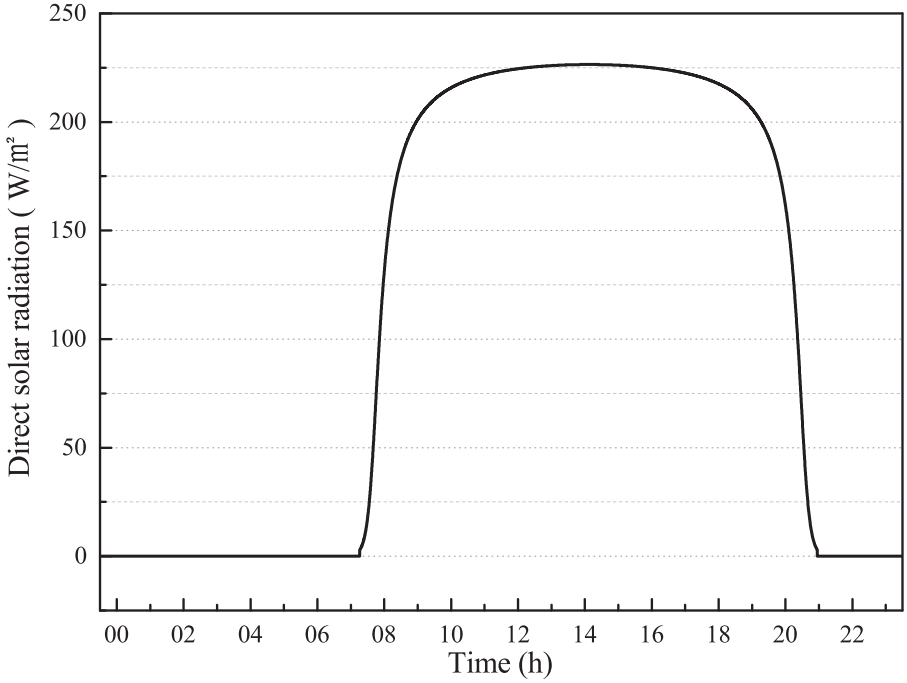

Fig. 10. Direct solar radiation at different time in one day with the altitude of 20 km.

speed is the mean value and the maximum differential pressure often occur at the end moment of the ascent phase, time delay exists between two curves in Fig. 9. And the length of the delay is about 45 min which is exactly half of the ascent phase.

4.2.3. *Influence of launch date*

The average rate of climb and the maximum differential pressure during ascent phase in different month of a year are presented in Fig. 11. The two main parameters show consistent seasonal variability. Due to the middle north latitude region is set as launch location in this simulation group, the average rate of climb and the maximum differential pressure reach maximum in summer (July), and reach minimum in winter (January). The average rate of climb in summer is higher than that in winter about 4.55%, and the maximum differential pressure in summer is higher than that in winter about 18.89%.

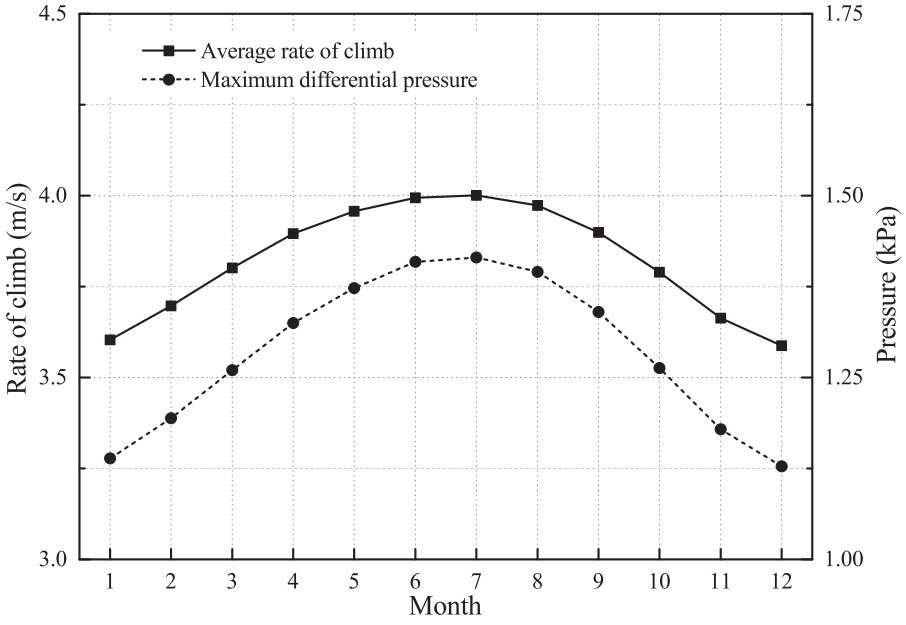

Fig. 11. Average rate of climb and maximum differential pressure in different month of a year.

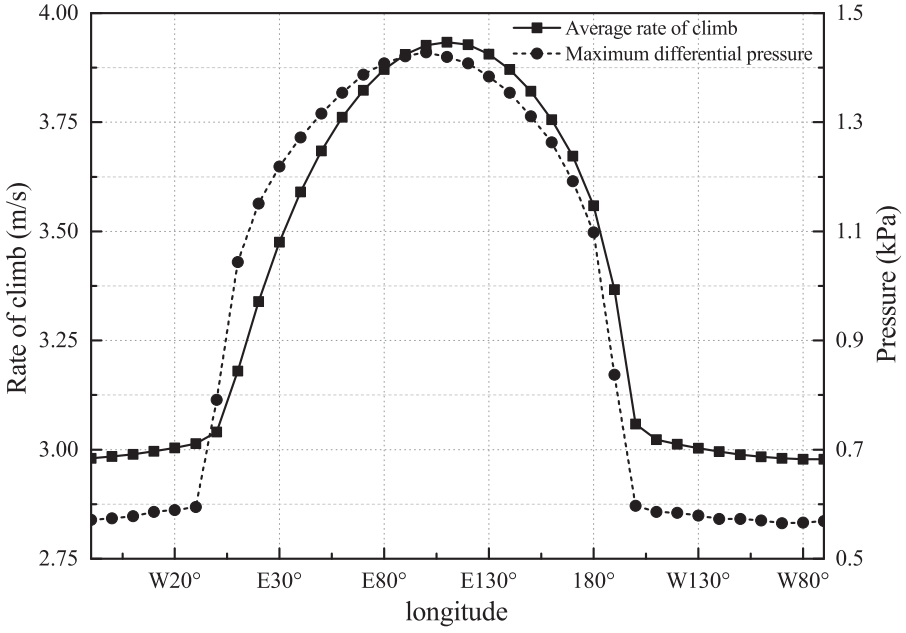

Fig. 12. Average rate of climb and maximum differential pressure with different launch longitude.

4.2.4. Influence of launch location

4.2.4.1. Influence of longitude. Due to the fact of earth rotation, the influence of changes in longitude is exactly same as changes in launch time which is indicated in Fig. 12. The starting time of the simulation data in Fig. 12 is set to 12:00 AM local time, and the peak values are recorded in the 116°E which is exactly where launch position is. And the distribution of the curve is in accordance with Fig. 9, it shows that the influence of longitude and launch time are same to ascent phase.

4.2.4.2. Influence of latitude. Due to the revolution of the Earth, the influence of changes in latitude is exactly same as changes in launch date which is indicated in Fig. 13. The starting time of the simulation data in Fig. 13 is set to 12:00 AM local time in September, and the peak values are recorded in the middle latitude region. The reason is that the middle latitude region in September is in summer and the intensity of solar radiation reaches its maximum. It shows that the influence of latitude and launch date are same.

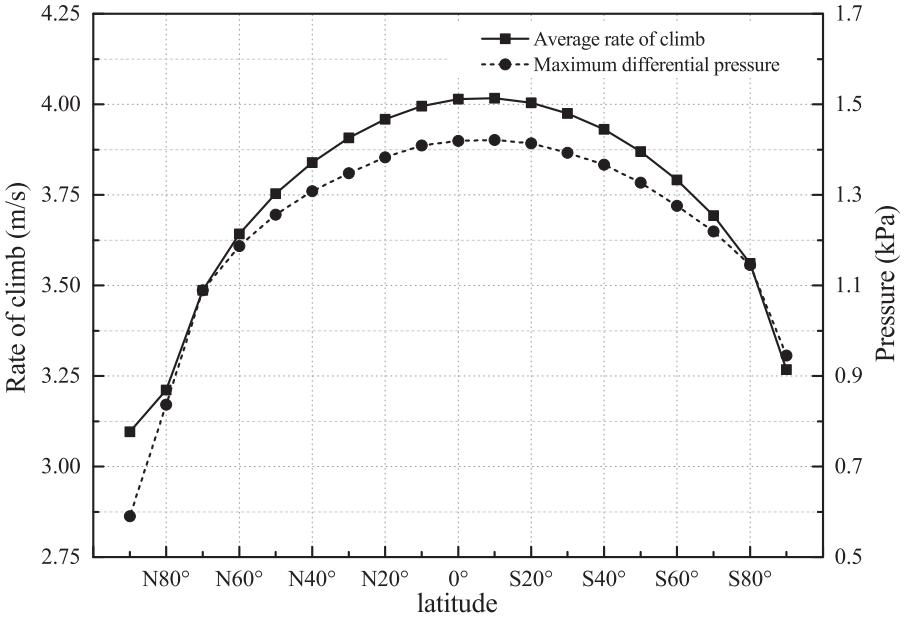

Fig. 13. Average rate of climb and maximum differential pressure with different launch latitude.

5. Conclusion

In this paper, we have investigated launch conditions effects on the flight performance of high altitude balloon during ascending. With radiation environment and balloon system description equations, a comprehensive numerical model was developed to investigate the detailed flight performances in different launch conditions. From the simulation results, the main conclusions are as follows:

1. Inflating quantity is the main factor that has influence on rising speed, and it is also the decisive factor of maximum differential pressure. A larger value of inflating quantity is required to increase rising speed on the premise of film strength safety.
2. In the daytime sufficient solar radiation can bring faster climbing rate, but meanwhile larger differential pressure will appear simultaneously. The best time for launch is at sunset, because solar energy can be used to accelerate and at the end of ascent phase solar radiation basically disappears which will lead to lower differential pressure.
3. In summer, both climbing rate and maximum differential pressure are larger than in winter. And they are at an intermediate level in spring and autumn. By comparison with launch time, launch date has less impact on two performance parameters.
4. The influence of launch position is same as launch time due to the fact of earth's rotation and revolution. Generally, limiting factors exist in the actual operation of launch site selection. Therefore, choice of launch time should be made with reference to launch point for making best use of sunset time quantum.

References

Agrawal, P.C., Sreenivasan, S., Subba Rao, J.V., 2002. Scientific ballooning in India. Adv. Space Res. 30 (5), 1117–1123.
Anderson, W.J., Taback, I., 1991. Oscillation of high-altitude balloons. J. Aircr. 28 (9), 606–608.
Carlson, L.A., Horn, W.J., 1983. New thermal and trajectory model for high altitude balloons. J. Aircr. 20 (6), 500–507.
Cathey Jr., H.M., 1996. Advances in the thermal analysis of scientific balloons. In: 34th Aerospace Sciences Meeting and Exhibit, Reno, USA.
Cathey Jr., H.M., 1997. Transient thermal loading of natural shaped balloons. In: International Balloon Technology Conference, USA.
Cathey Jr., H.M., 2009. The NASA super pressure balloon A path to flight. Adv. Space Res. 44 (1), 23–38.
Cho, C., Raque, S., 2002. Influence of the infrared radiation on a high altitude scientific balloon. In: 40th AIAA Aerospace Sciences Meeting & Exhibit, USA.
Conner Jr., J.P., Arena Jr., A.S., 2010. Near space balloon performance predictions. In: 48th AIAA Aerospace Sciences Meeting Including the New Horizons Forum and Aerospace Exposition, Florida, USA.
Dai, Q.M., Fang, X.D., Li, X.J., Tian, L.L., 2012. Performance simulation of high altitude scientific balloons. Adv. Space Res. 49 (6), 1045–1052.
Farley, R.E., 2005. BalloonAscent: 3-D simulation tool for the ascent and float of high-altitude balloons. In: AIAA 5th ATIO and 16th Lighter-Than-Air Sys Tech. & Balloon Systems Conferences, Virginia, USA.
Franco, H., Cathey Jr., H.M., 2004. Thermal performance modeling of NASA's scientific balloons. Adv. Space Res. 33 (10), 1717–1721.
Germeles, A.E., 1966. Vertical motion of high altitude balloons. AD485401.
Guo, X., Zhu, M., 2013. Ascent trajectory optimization for stratospheric airship with thermal effects. Adv. Space Res. 52 (6), 1097–1110.
Kreith, F., Kreider, J.F., 1974. Numerical prediction of the performance of high altitude balloons. In: Atmospheric Technology Division, National Center for Atmospheric Research.
Liu, Q., Wu, Z., Zhu, M., Xu, W.Q., 2014. A comprehensive numerical model investigating the thermal-dynamic performance of scientific balloon. Adv. Space Res. 53 (2), 325–338.
Makino, F., 2002. Scientific ballooning in Japan. Adv. Space Res. 30 (5), 1095–1104.

Morani, G., Palumbo, R., Cuciniello, G., Corraro, F., Russo, M., 2009. Method for prediction and optimization of a stratospheric balloon ascent trajectory. J. Spacecraft Rockets 46 (1), 126–133.

Mueller, J., Paluszek, M., Zhao, Y., 2004. Development of an aerodynamic model and control law design for a high altitude airship. In: AIAA 3rd Unmanned Unlimited Technical Conference, Workshop and Exhibit, USA.

Palumbo, R., Russo, M., Filippone, E., Corraro, F., 2007. ACHAB: analysis code for high-altitude balloons. In: AIAA Atmospheric Flight Mechanics Conference and Exhibit, South Carolina, USA.

Palumbo, R., Morani, G., Corraro, F., 2010. Effective approach to characterization of prediction errors for balloon ascent trajectories. J. Aircr. 47 (4), 1331–1337.

Pankine, A.A., Heun, M.K., Schlaifer, R.S., 2003. Advanced balloon performance simulation and analysis tool. In: AIAA's 3rd Annual Aviation Technology, Integration, & Operations (ATIO) Forum, USA.

Ran, H.J., Thomas, R., Mavris, D., 2007. A comprehensive global model of broadband direct solar radiation for solar cell simulation. In: 45th AIAA Aerospace Sciences Meeting and Exhibit, Nevada, USA.

Schmidt, D.K., Stevens, J., Roney, J., 2007. Near-space station-keeping performance of a large high-altitude notional airship. J. Aircr. 44 (2), 611–615.

Smith Jr., I.S., 2004. The NASA balloon program: looking to the future. Adv. Space Res. 33 (10), 1588–1593.